
Delay Conditioned Generative Modelling of Resistive Drift in Memristors

Waleed El-Geresy
Imperial College London
waleed.el-geresy15@imperial.ac.uk

Christos Papavassiliou
Imperial College London
c.papavas@imperial.ac.uk

Deniz Gündüz
Imperial College London
d.gunduz@imperial.ac.uk

Abstract

The modelling of memristive devices is an essential part of the development of novel in-memory computing systems. Models are needed to enable the accurate and efficient simulation of memristor device characteristics, for purposes of testing the performance of the devices or the feasibility of their use in future neuromorphic and in-memory computing architectures. The consideration of memristor non-idealities is an essential part of any modelling approach. The nature of the deviation of memristive devices from their initial state, particularly at ambient temperature and in the absence of a stimulating voltage, is of key interest, as it dictates their reliability as information storage media - a property that is of importance for both traditional storage and neuromorphic applications. In this paper, we investigate the use of a generative modelling approach for the simulation of the delay and initial resistance-conditioned resistive drift distribution of memristive devices. We introduce a data normalisation scheme and a novel training technique to enable the generative model to be conditioned on the continuous inputs. The proposed generative modelling approach is suited for use in end-to-end training and device modelling scenarios, including learned data storage applications, due to its simulation efficiency and differentiability.

1 Introduction

Memristors are a class of passive electronic device that have a semi-volatile resistive state (memory) which can be modified through the application of a driving voltage or current. The memristor was originally hypothesised by Leon Chua [Chua, 1971] as the missing fundamental passive circuit element in a “periodic table” of passive electronic devices. Later, the definition and scope of the term “memristor” expanded to encompass a variety of resistive switching technologies [Chua, 2014, Chua, 2011], and the definition as used nowadays in literature on the subject is more or less interchangeable with the term “memristive systems” [Chua and Sung Mo Kang, 1976] - a generalisation of the original definition. Notable types of device that have been described as “memristive” include phase change memory devices and thin film metal oxide devices. The possible uses of memristors go beyond information storage and extend to the realm of so-called neuromorphic computing [Sung et al., 2018], where computation and storage occur at the same physical location, and thus, in a distributed and massively parallelised way [Mead, 1990].

Due to their promising potential applications, building useful models of memristive devices has become a subject of interest. One particular problem is that of modelling the noise and stochasticity (the non-deterministic components) of device behaviour.

The problem of building effective models of memristive devices has been previously addressed using both deterministic [Strukov et al., 2008, Pickett et al., 2009, Yang et al., 2008] and stochastic approaches [Molter and Nugent, 2016, Malik et al., 2022]. Modelling considerations include the computational complexity, the accuracy, and the explainability (physical realism and grounding) of the model [Williams et al., 2013]. In order to provide models that are minimally computationally intensive, but also accurate, we must take into account the intended application. This also has a bearing on the range of applications for the model. For example, models may be written in SPICE to allow for simulation alongside existing analogue circuitry [Berdan et al., 2014] and more recently, a model intended for event-based neuromorphic computing applications has been proposed [El-Geresy et al., 2024].

In the context of deep learning and artificial intelligence (AI), data-driven approaches to modelling - known as generative modelling approaches - are becoming increasingly popular due to their ability to learn to simulate complex data with minimal assumptions on the nature of the underlying distribution. The popularity of generative modelling techniques has been fuelled by recent impressive results in the conditional generation of realistic data in a variety of modalities, such as natural language, images, and video.

In this work, we develop a generative modelling technique for the modelling of one particular kind of memristive non-ideality: resistive drift. Although a variety of non-idealities plague memristive devices [Rumsey, 2019, Oh et al., 2019, Zarcone et al., 2020], resistive drift noise is unique in that it is sequential in time; that is, it has temporal correlations. Resistive drift describes the phenomenon of the stochastic decay of the state of a memristive device over time, until an equilibrium resistance is attained and all information about the original storage values is lost [Ielmini, 2011, El-Geresy et al., 2024]. The problem of modelling resistive drift deterministically has been previously addressed through methods including modelling that incorporates autonomous state evolution [Carbajal et al., 2015], and modelling of the resistive drift using a stretched exponential function [Abbey et al., 2022]. Modelling approaches that take into account the stochastic nature of the state transitions have also been proposed [Malik et al., 2022, El-Geresy et al., 2024], though so far, generative modelling approaches have not been explored.

1.1 Time Series Generative Modelling

The temporal correlations and dependencies present in time series data present a unique challenge that require specialised time series generative modelling techniques. Time series generative models come in a variety of forms. They can be either recurrent, or non-recurrent, and they can be either deterministic or stochastic.

Recurrent architectures make use of stateful neural networks such as Long Short-Term Memory (LSTM) cells [Hochreiter and Schmidhuber, 1997] or Gated Recurrent Units (GRUs) [Cho et al., 2014], which use a state variable to capture dependencies between elements of the series over time. Challenges associated with generating time series using Recurrent Neural Network (RNN) architectures also include the computational complexity of the model, with many subsequent sampling steps leading to a large number of forward passes, if the recurrent architecture is unrolled. This increases the computational complexity of the generation of a data sample, and also means that the network is prone to vanishing gradient issues during training, or if used as a fixed differentiable model in an end-to-end training setup.

Alternatively, finite-memory time series generation can be achieved through the use of autoregressive architectures [van den Oord et al., 2016], which generate values based on a fixed horizon of past inputs. Despite the effectiveness of autoregressive models, they are fundamentally deterministic, being functions of past inputs. In addition, while such models can generate a future value, or sometimes sequences, in a single step, they must be recurrently evaluated on previously generated data to generate values beyond this.

Problems in training both types of time series models may arise due to the disconnect between so-called “closed-loop” training and “open-loop” evaluation [Yoon and Jarrett, 2019], where the contrast between evaluation of the model in a recurrent manner during inference, as opposed to

its conditioning on previous ground truth data values during training, may cause problems with distributional mismatch. Several methods exist for addressing this problem, notably the use of scheduled sampling (a form of curriculum learning), involving a gradual transition between open-loop training and closed-loop training [Bengio et al., 2015]. It has however been suggested that techniques such as scheduled sampling are alone insufficient for addressing this problem [Yoon and Jarrett, 2019], with the technique also being criticised for memorisation of samples [Huszár, 2015].

1.2 Contributions and Outline

In this paper, we employ a generative modelling approach to learn a differentiable model of the resistive drift, conditioned on two continuous conditions: an initial resistance value and a delay. The use of generative modelling to simulate the resistive drift has the advantage of being purely data driven, and allows us to model the drift over time in a computationally efficient manner, creating a differentiable model that is suitable for use in deep learning frameworks. We propose a computationally simple approach to single-shot generation, which additionally reduces problems associated with vanishing gradients which would be present for models involving recurrence. We condition directly on the delay rather than recurrently evaluating. As such, our contributions can be summarised as follows:

1. We investigate methods for data normalisation in the context of time series data with a continuous, high dynamic range for the model input and output values. Conditioning Generative Adversarial Networks (GANs) on continuous values has previously been investigated [Ding et al., 2022], although in the context of resistive drift, the large dynamic range for time and resistance inputs and resistance outputs presents a particular challenge.
2. We present an approach to conditioning generative models directly on the delay that exploits the temporal structure of time series data to enforce consistency in time series outputs generated at different timescales. Traditional time series generative models are fixed in the timescales at which they generate time series data; that is, they generate time series data of fixed intervals, say Δ . Therefore, to generate a sample at time $t + k \cdot \Delta$, the model is run k times in a recursive fashion. We introduce a novel adversarial training technique, which we call *delay discrimination*, to enable us to generate time series data at a range of timescales with consistency. By conditioning the model on the delay, we avoid the need for many recurrent evaluations of the model, making it computationally efficient. This minimisation or elimination of additional recurrent inference steps also thus alleviates problems caused by the disconnect between closed-loop training and open-loop evaluation. Our method also allows the model to generate outputs at arbitrary continuous delay values, rather than being constrained to generate values at integer multiples of the timestep.
3. We demonstrate the benefits and effectiveness of the proposed model in end-to-end training settings, detailing its use in a learned approach to the problem of quantised data storage and recovery on memristors.

In Section 2, we describe the process and motivation behind the creation of an example resistive drift dataset, used to train and evaluate our proposed approach. We make use of a general stochastic memristor model for the creation of the dataset [El-Geresy et al., 2024]. In Section 3, we introduce the proposed conditional Generative Adversarial Network (cGAN) training procedure and methods, including the novel approach of delay discrimination, which is used to enable our network to learn to generate outputs conditioned on a wide range of delays. We present the model fitting results and a discussion of the performance of our method in Section 4. Finally, in Section 5, we demonstrate the use of our modelling approach in the problem of the design of an end-to-end optimised, low-error quantisation scheme, demonstrating the benefits of its computational efficiency and efficacy in a realistic problem.

Notation Throughout this paper, we use $BCE(y, \hat{y}) \triangleq (y - 1) \ln(1 - \hat{y}) - y \ln(\hat{y})$ to represent the Binary Cross-Entropy (BCE) function. In general, we use lowercase r to denote resistance values, d to denote delay values, and \bar{y} to denote a normalised version of a given variable y . $N_x(\cdot)$ is used to denote a particular data normalisation transform.

Table 1: The parameters used for generation of the simulated resistance drift dataset, with an equilibrium resistance of $500k\Omega$. For a full description of the model used to generate the dataset, please see [El-Geresy et al., 2024].

Parameter	Definition	Value
N	The number of metastable switches, dictating the granularity of simulation.	1.8×10^6
n_{thresh}	The threshold for the resistance readout equation.	0
V_a	The energy barrier height, dictating absolute switching rate.	0.256
g_{parallel}	The low conductance in the readout equation.	1×10^{-6}
g_{step}	The marginal conductance increase in the readout equation.	$\frac{1 \times 10^{-2}}{1 \times 10^6}$
V_{off}	The offset voltage dictating the equilibrium offset.	0.2532
T	The bath temperature.	300
k_B	Boltzmann’s constant.	1.38064×10^{-23}
q	The electronic charge.	1.602176×10^{-19}

2 Resistive Drift Dataset

We make use of the titanium dioxide memristor model developed in [El-Geresy et al., 2024] to model resistive drift in a simulated, highly stochastic memristive device. We generate a dataset consisting of 5000 drift time series. We choose a set of parameters that result in relatively unstable device characteristics, presenting a relatively extreme and challenging modelling scenario, where decay to an equilibrium resistance point happens at a rapid rate.

2.1 Parameter Selection and Dataset Creation

We choose the parameter V_a , which controls the rate of switching, to yield a drift distribution with sufficient variation and stochasticity over the interval of interest of 1000s. We choose the parameters N , n_{thresh} , g_{step} , and g_{parallel} to allow for a sufficiently fine description of the states over the resistance interval $[0.1k\Omega, 100k\Omega]$: our chosen active switching region. We choose our equilibrium point to be approximately $500k\Omega$, corresponding to $n = 100$ according to the chosen parameters and the chosen readout equation, mimicking the one developed for the titanium dioxide memristor in [El-Geresy et al., 2024]:

$$R(n) = \frac{1}{g_{\text{diff}} \max(n, n_{\text{thresh}}) + \frac{1}{R_{\text{high}}}} \quad (1)$$

We set V_{off} accordingly to achieve this, using Equation 2, as derived in [El-Geresy et al., 2024]. Using a value of $n_{eq} = 100$ along with the chosen value of $V_a = 0.256$, in order to adjust the stability/speed of convergence, gives a required value of $V_{\text{off}} = 0.2533$ to achieve the necessary equilibrium state.

$$V_{\text{off}} = \ln \left(\frac{N - n_{eq}}{n_{eq}} \right) \cdot \frac{k_B T}{q} \quad (2)$$

For the given V_{off} , we invert the equation to calculate the error in our equilibrium point: we can see that this yields gives a true equilibrium value of $n_{eq} = 100.38$, corresponding to a resistance of $R_{eq} = 499.076k\Omega$, which is sufficiently close to the desired value of $500k\Omega$.

A summary of the physical parameters and constants chosen for generation of the data are given in Table 1.

We generate 5000 time series with initial points spaced uniformly in the range $[100\Omega, 750k\Omega]$. For each generated series, we sample the data uniformly, with timestep $T_{\text{sample}} = 1$ and total series duration $T_{\text{tot}} = 1000$, resulting in 1001 data points in each series, spaced one second apart (inclusive of points at $t = 0$ and $t = T_{\text{tot}}$).

2.2 Dataset Visualisation and Evaluation

A sampled subset of the series in the resistive drift dataset are shown in Figure 1. We also show the output time series of the proposed model for the same initial resistance conditions for comparison.

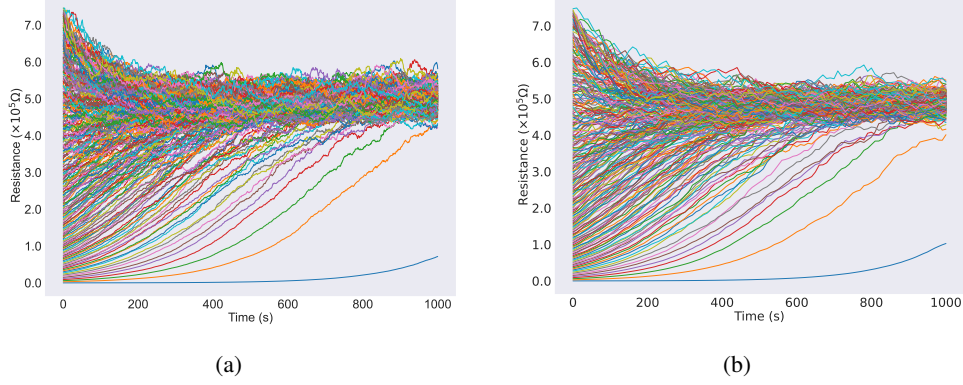


Figure 1: **Left:** An illustrative subset of the time series dataset used for training the cGAN, generated using the event-based model of [El-Geresy et al., 2024]. It clearly illustrates the stochasticity of the resistance values, and their convergence to the equilibrium point of $500k\Omega$. The variance of the state transitions increases with increasing initial resistance. **Right:** The proposed modelling approach evaluated on the same initial resistances for a timestep of 10 and a series length of 100 (a total delay of 1000). It is clear that the model is able to approximate the conditional drift distribution.

The distribution of final resistance values across the dataset is shown in Figure 2. We can see that over the course of 1000 seconds, almost all series converge to lie within a small region surrounding the equilibrium resistance of $500k\Omega$. This demonstrates that the information capacity of the device is a function of the delay, and decreases over time. Due to the drift towards the equilibrium point, all the information stored in the device will eventually be lost. According to the modelling parameters chosen, the energy imbalance between the rates of switching in the positive and negative directions, modulated by V_{off} (see [El-Geresy et al., 2024])), results in an equilibrium resistance of $500k\Omega$, and thus, favours drift in the direction of the high resistance for resistances in the range chosen for the dataset. This stochastic deviation of the resistance from its initial point is the distribution that we wish to model using the cGAN.

3 Conditional GAN (cGAN) Training

In this section, we introduce our approach to modelling the delay and initial resistance conditional distribution of resistance drift in memristors, through the use of time series generative modelling. Letting $r(t)$ denote the resistance as a random process, with t representing the time, our goal is as follows: we wish to find a computationally efficient and differentiable model that given an initial resistance value $r(0)$ and a given delay d , parameterises the conditional distribution $p(r(d)|r(0), d)$.

3.1 Delay Discriminator

As mentioned in Section 1.1, several types of generative models have been proposed for modelling time series data. However, one major disadvantage to these approaches is that their output for a given timescale is fixed; this results in the need for recurrent evaluation of the models during inference. Thus the distribution $p(r(d)|r(0), d)$ is decomposed into the factorised distribution based on the sampling step ΔT of the time series generative model:

$$p(r(d)|r(0), d) = \prod_{i=0}^{(d/\Delta T)-1} p(r((i+1) \cdot \Delta T) | r(i \cdot \Delta T)) \quad (3)$$

Since the purpose of our model is to be used as a proxy for a physical imperfection in an end-to-end differentiable learning setup, it is desirable to have a model that is as computationally simple and shallow (in terms of layers) as possible. The decomposition of the sampling into many steps can be both computationally demanding and can subsequently result in vanishing gradient issues in

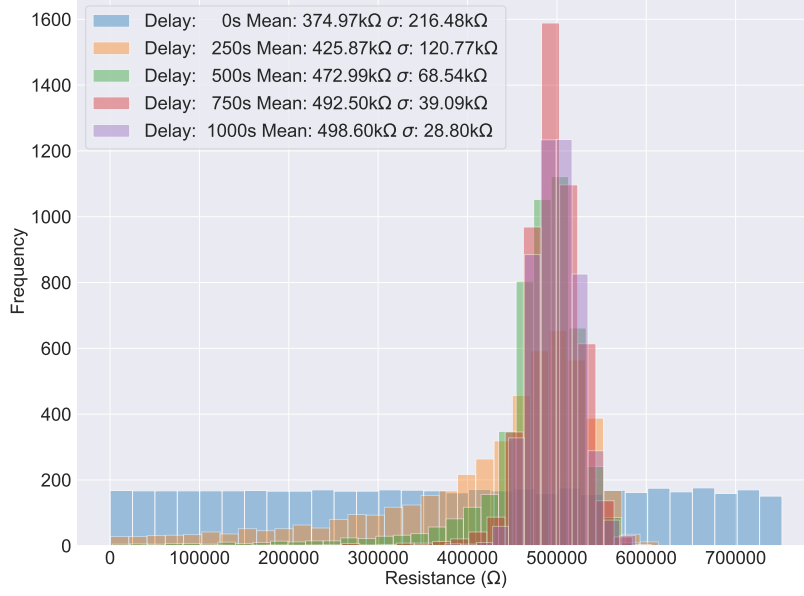


Figure 2: Histogram of final resistance values in the drift dataset at different delays. We see that as the delay increases to 1000s, the distribution becomes centred around the equilibrium resistance value - i.e. any information present in the encoding of the initial value is lost. The legend shows the mean value for each delay conditioned distribution, μ , and the standard deviation, σ .

end-t-end settings. Additionally, if not appropriately addressed during training, issues can arise from a disconnect between closed-loop training and open-loop evaluation.

To address these problems, we propose to modify our generative modelling approach with the introduction of an additional condition: the delay, such that the final output, $r(d)$, can be obtained directly by sampling the model output, that is - computing $p(r(d) | r(0), d)$ directly. This will proffer several key advantages in our setting, and more generally:

1. **Computational efficiency:** by conditioning directly on the delay, we are able to avoid the need for computationally expensive recurrent evaluation in order to generate outputs for larger delays. This reduction in computational complexity can also improve the flow of gradients through the model (fewer layers) when it is used in an end-to-end training setting.
2. **Larger delays:** The model is able to learn to generate outputs conditioned on larger delays, by enforcing consistency with recurrent model output at smaller delays.
3. **Addressing the disconnect between closed-loop training and open-loop evaluation:** By heavily reducing the need to recurrently run the model during inference, we minimise the possibility for open-loop evaluation errors to be introduced.

Conditioning on the delay directly introduces additional complexity to our modelling problem, and makes it more difficult to train the model. To address this, we introduce a novel approach for enforcing consistency between time series generated at different resolutions, called delay discrimination. The adversarial approach relies on enforcing consistency in the generation of the outputs of the model, for the same total delay, evaluated at different timescales through an adversarial approach, where the model’s own outputs at different scales are compared to one another (see Figure 7).

We introduce a novel approach called *delay discrimination*, which makes use of a network we call the *delay discriminator*. This is an auxiliary discriminator network trained alongside the main generative model, forming an additional GAN, with our generative model acting as the generator. We use this to improve the ability of the generative model to condition on the continuous delay conditions present in (that can be generated from) the training data, and also to improve the performance for larger delay conditions, outside of those available in the original training dataset.

Algorithm 1 Algorithm for updating the network parameters of the generator and delay discriminator for a single batch of size b . α is the learning rate.

```

1:  $q \sim U\{2, q_{\max}\}$ 
2:  $\mathcal{P}_{dd,1} \leftarrow \{\}$ 
3:  $\mathcal{P}_{dd,2} \leftarrow \{\}$ 
4: for  $i \in b$  do
5:    $d_{dd} \in U\{d_{\min,dd}, d_{\max,dd}\}$ 
6:    $r_{\text{init}} \leftarrow U\{R_{\min}, R_{\max}\}$ 
7:    $r_{\text{final},1} = G_{\theta_g}(r_{\text{init}}, d_{dd})$ 
8:    $r_{\text{final},2} \leftarrow r_{\text{init}}$ 
9:   for  $j \in q$  do
10:     $r_{\text{final},2} \leftarrow G_{\theta_g}(r_{\text{init}}, d_{dd}/q)$ 
11:     $\mathcal{P}_{dd,1} \leftarrow \mathcal{P}_{dd,1} \cup D_{dd;\theta_{dd}}(r_{\text{init}}, r_{\text{final},1})$ 
12:     $\mathcal{P}_{dd,2} \leftarrow \mathcal{P}_{dd,2} \cup D_{dd;\theta_{dd}}(r_{\text{init}}, r_{\text{final},2})$ 
13:  $\theta_{dd} \leftarrow \theta_{dd} + \alpha \nabla_{\theta_{dd}}(BCE(\mathcal{P}_{dd,1}, \{0, \dots, 0\})) + \alpha \nabla_{\theta_{dd}}(\mathcal{P}_{dd,2}, \{1, \dots, 1\})$ 
14:  $\theta_g \leftarrow \theta_g + \alpha \nabla_{\theta_g}(BCE(\mathcal{P}_{dd,1}, \{1, \dots, 1\}))$ 

```

We base our method on the inductive bias that a network conditioned on the delay should generate the same output distribution, regardless of the delay value, if evaluated recurrently, so long as the total delay is the same. For example, the network should generate the same conditional output distribution for a given initial resistance if it is conditioned directly on a total delay of 10, say, or if it used in a recurrent fashion for 10 iterations with a delay of 1. The delay discrimination algorithm is shown in Algorithm 1 for a batch size of b , where $D_{dd;\theta_{dd}} : \mathbb{R}^2 \rightarrow [0, 1]$ represents the delay discriminator mapping, parameterised by θ_{dd} .

The principle is to train an auxiliary GAN discriminator network to differentiate between the final values of two model series trained for different timescales. We first randomly generate a discriminator delay in the range $d_{dd} \in [d_{ddmin}, d_{ddmax}]$, where $d_{ddmin} > 0$ and $d_{ddmax} \geq d_{max}$, as well as a random integer factor in the range $q \in \{2, \dots, q_{max}\}$. We then condition the generative model on the delay d_{dd} , and given a randomly selected resistance r_{dd} as the initial condition, generate a single sample. Since this sample is generated with no reference to previously generated samples, it does not suffer from closed loop errors. Following this, we generate q samples using the generator, with a delay condition of d_{dd}/q . We discard all but the conditioning resistance and the last sample for this second generated series. The delay discriminator, $D_{dd;\theta_{dd}}$, is trained to distinguish between final sample of the recurrent, open-loop evaluation for the smaller delay, and the sample generated using a single (non-recurrent) generation step for the larger delay. The result of this training process is to cause the generative model to change its generation of the series of delay d to be more akin to the series with delay d/q , and vice versa. The procedure for training the delay discriminator is shown in Algorithm 1. In practice, we use a value larger than 1. Delay discrimination benefits the training in several ways:

1. Information from the closed-loop evaluation for larger delays passes through to condition the open-loop evaluation for smaller delays, allowing inconsistencies to be highlighted and connecting the two forms of evaluation.
2. Inclusion of the delay consistency inductive bias reduces training complexity and improves convergence.
3. It allows data to be generated with delays larger than present in the dataset, as well as fractional delays, allowing for a much wider range of delays to be used for conditioning the generator in the training process. Following training, the generator can model the conditional distribution after much larger delays, without many recurrent evaluation steps.

We will highlight the effectiveness of the delay discriminator method in Section 4.2, where we look at the mean and variance of the values after an equivalent total delay of 1000 for series generated using delay conditions in the set $[5, 10, 100, 250, 1000]$. We will demonstrate that using the delay discriminator vastly improves consistency of generation, especially for larger delays.

3.2 Data Transformation and Normalisation

For any data-driven optimisation problem, it is important to appropriately transform the input data, in order to incorporate known inductive biases that facilitate learning. It is also well-known that data normalisation aids the learning process by ensuring that there is no bias in the contribution of features to the gradients of the network during optimisation.

The nature of our input features - the initial resistances and the delays - presents a challenge to our learning algorithm, due to their domain spanning multiple orders of magnitude. We must choose an appropriate data transformation that reduces the large range, while also allowing for precision in generation at a variety of scales.

In the case of the normalisation of the resistance values, we apply a logarithmic transform followed by subtraction of the mean and scaling by the standard deviation (using statistics empirically averaged over the drift dataset) in order to normalise the magnitudes. We determine the parameter μ_R as the sample mean of the logarithmically transformed resistances, taken over the dataset, and similarly find σ_R as the square root of the sample variance of the resistances present in all resistance series, S_i - indexed by i , in the dataset, \mathcal{D} :

$$\begin{aligned}\mu_R &= \frac{1}{|\mathcal{D}|} \sum_{S_i \in \mathcal{D}} \frac{1}{|S_i|} \sum_{r_j^i \in S_i} \ln(r_j^i), \\ \sigma_R &= \sqrt{\frac{1}{|\mathcal{D}|} \sum_{S_i \in \mathcal{D}} \frac{1}{|S_i|} \sum_{r_j^i \in S_i} (\ln(r_j^i) - \mu_R)^2},\end{aligned}\quad (4)$$

where $r_j^i \in S_i$ are the ordered (resistance) elements of the series S_i , indexed by j . Thus, the resistance normalisation transformation, $N_{\text{res}}(r)$, is given as:

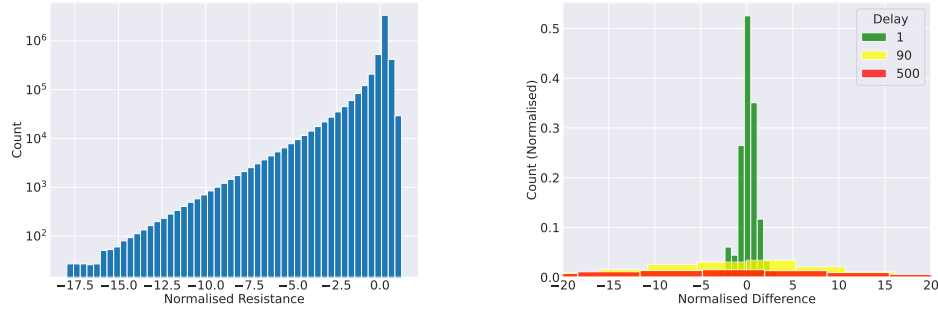
$$N_{\text{res}}(r) = \frac{\ln(r) - \mu_R}{\sigma_R} \quad (5)$$

We found that it was more efficient to train the generator network to predict the differences in the normalised resistance values, rather than the absolute values. As such, we apply a residual connection [He et al., 2016] between the input and the output. Prediction of the difference incorporates the inductive bias that the output should be equal to the input by default for a value of 0. This inductive bias is a common feature of popular neural network architectures, such as U-Net [Ronneberger et al., 2015] or multi-head attention modules in transformers [Vaswani et al., 2017], which use residual connections.

To normalise the differences of the normalised dataset, we apply a conditional mapping - $N_{\text{diff}}(\cdot, \cdot)$ - that is dependent on both the normalised input resistance, $\bar{r}_{\text{init}} = N_{\text{res}}(r_{\text{init}})$, and the normalised output resistance, $\bar{r}_{\text{final}} = N_{\text{res}}(r_{\text{final}})$, resulting in the normalised difference, denoted by \bar{r}_{diff} . Note that the difference normalisation transform is applied atop data normalisation. Let $\bar{\mathcal{D}}$ denote the normalised dataset, created by applying $N_{\text{res}}(\cdot)$ pointwise to all $r_j^i \in S_i \forall S_i \in \mathcal{D}$. We denote the series of the normalised dataset as $\bar{S}_i \in \bar{\mathcal{D}}$ and the resistance values in each normalised series as $\bar{r}_j^i \in \bar{S}_i$. The forward (Equation (7)) and inverse (Equation (6)) difference normalisation transforms are defined as follows, with the standard deviation used for normalisation calculated from the dataset statistics for a delay of 1:

$$\begin{aligned}\mu_{\bar{\mathcal{D}}} &= \frac{1}{|\bar{\mathcal{D}}|} \sum_{\bar{S}_i \in \bar{\mathcal{D}}} \frac{1}{|\bar{S}_i| - 1} \sum_{\{\bar{r}_j^i \in \bar{S}_i | j < |\bar{S}_i|\}} (\bar{r}_{j+1}^i - \bar{r}_j^i) \\ \sigma_{\bar{\mathcal{D}}} &= \sqrt{\frac{1}{|\bar{\mathcal{D}}|} \sum_{\bar{S}_i \in \bar{\mathcal{D}}} \frac{1}{|\bar{S}_i| - 1} \sum_{\bar{r}_j^i \in \bar{S}_i} (\bar{r}_j^i - \mu_{\bar{\mathcal{D}}})^2} \\ N_{\text{diff}}^{-1}(\bar{r}_{\text{diff}}, \bar{r}_{\text{init}}) &= \bar{r}_{\text{init}} + \bar{r}_{\text{diff}} \cdot \sigma_{\bar{\mathcal{D}}}\end{aligned}\quad (6)$$

$$N_{\text{diff}}(\bar{r}_{\text{final}}, \bar{r}_{\text{init}}) = \frac{(\bar{r}_{\text{final}} - \bar{r}_{\text{init}})}{\sigma_{\bar{\mathcal{D}}}} \quad (7)$$



(a) Histogram of the normalised resistances, obtained by applying the transform $N_{\text{Res}}(\cdot)$ pointwise to the resistance values in the series in the dataset D . (b) Normalised histograms for the differences, for a range of delay conditions, derived empirically from the dataset D , obtained by applying the difference normalisation transform $N_{\text{diff}}(\cdot, \cdot)$ to the pairs of values separated by delay ΔT .

Figure 3: Histograms of the values in the dataset, D following the initial pointwise application of the resistance normalisation transform (Figure 3a) and subsequent application of the difference normalisation transform for pairs of values from the dataset separated by a given delay (Figure 3b).

Figure 3 shows the distribution of values following the application of the resistance normalisation and difference normalisation transforms to the resistances in the dataset. In both cases, the normalisation transforms map the data to a more reasonable input range, while also retaining precision in their descriptive capabilities at different orders of magnitude. Note that, in the case of the difference normalisation transform, larger delays result in a larger range of values observed in the transformed histogram. It is also possible to ensure that the histograms are limited in their range by incorporating delay scaling in the difference normalisation transform; however, we found that retaining the different ranges of the transformed resistances for different delay conditions actually improved the training performance.

Similarly, despite the large range of delays used for training, denoted by $[d_{\min}, d_{\max}]$ with $d_{\min} = 1$ and $d_{\max} = 500$, it was found that scaling of the delays using a logarithmic transform did not benefit training. This is likely due to the magnitude of the normalised differences (the feature that the generator is trained to predict) being somewhat proportional to the delay condition. Thus, we apply no transformation to the delays and pass the unscaled delays directly to the network.

3.3 cGAN Generative Model

GANs are generative models that have been shown to be capable of effectively modelling complex distributions through the use of adversarial training [Goodfellow et al., 2014]. We will use a conditional form of GANs, called cGANs [Mirza and Osindero, 2014], where the generator parameterises the delay and initial resistance conditioned resistive drift distribution. Time Series GAN is one GAN that has shown success in generating realistic time series data [Yoon and Jarrett, 2019]; however, the model still requires recurrent evaluation for the generation of time series values at arbitrary points in the future.

We use a canonical BCE loss for the discriminator for our GAN training. We denote the generator network as G_{θ_g} , parameterised by θ_g ; and we denote the main discriminator network as $D_{d;\theta_d}$, parameterised by θ_d [Goodfellow et al., 2014]. Let us denote the distribution induced by sampling from G_{θ_g} as $p_f(f)$, and the ground truth data distribution as $p_x(x)$. Our discriminator objective is the maximisation of the likelihood of classifying samples as 1, or “real”, when evaluated on real data samples, and the simultaneous maximisation of the likelihood of classifying samples as 0, or “fake”, when evaluated on the distribution induced by the generator. This is achieved by the discriminator’s minimisation objective:

$$L_{\theta_d} = -\mathbb{E}_{x \sim p_x(x)}[\log(D_{d;\theta_d}(x))] - \mathbb{E}_{f \sim p_F(f)}[\log(1 - D_{d;\theta_d}(f))] \quad (8)$$

Our generator objective is to maximise the likelihood of the discriminator classifying samples generated from the induced distribution as 1, or “real”. This is achieved by the generator’s minimisation objective being:

$$L_{\theta_d} = -\mathbb{E}_{x \sim p_x(x)}[\log(D_{d;\theta_d}(x))] \quad (9)$$

Wasserstein GAN proposes an alternative optimisation objective, requiring the use of the associated techniques of discriminator weight or gradient clipping to enforce the Lipschitz constraints on the discriminator [Arjovsky et al., 2017]. However, we found that for our problem setting, the original GAN loss function as described in Equations (8) and (9) above, yielded better convergence.

3.4 Training Details

3.4.1 Architecture

We use a modular, fully connected architecture, with ReLU non-linear activation functions for both the generator and the discriminator. We observed that, in practice, using batch normalisation in the generator network harmed the performance. A diagram showing the network architecture for the generator network is shown in Figure 4. The discriminator network architecture is shown in Figure 5. A network diagram, showing the overall training procedure, including both the discriminator and the auxiliary delay discriminator, is shown in Figure 6.

3.4.2 Feeding Data to the Network

We train in a mixed-mode setup, with the normalised initial resistance condition being passed as an initial value and the subsequent values fed recurrently back to the network to generate further samples of the series. Once a sequence of $s - 1$ additional values have been recurrently generated by the generator network, the entire generated sequence is fed simultaneously to the discriminator. This ensures that both open-loop and closed-loop errors (see Section 1.1) are used simultaneously to update the network parameters, allowing for the network to be used recurrently if needed during evaluation.

We experimented with the choice of which transformed versions of the input to pass to each of the networks - the generator and the discriminator(s). We found that presenting a vector consisting of both the normalised resistances, \bar{r}_{init} , and the normalised differences, \bar{r}_{diff} , to the discriminator improved the performance. The normalised resistances can be seen as providing information about the absolute value of the input (the order of magnitude), while the normalised differences provide more fine-tuned information about the relative values. The discriminator is fed a series of s normalised resistance values simultaneously, along with a series of $s - 1$ normalised difference values, that are obtained by computing the difference normalisation transform of the pairs of resistance values. The first element of the resistance series fed to the discriminator is always a real datapoint, and the other $s - 1$ values are either the remainder of the series generated from the training set, or $s - 1$ generated values. The output of the discriminator is a real number in the range $[0, 1]$ representing its belief that the given resistance and delay values were drawn from the dataset (1) or that they were generated (0). The dimensionality and the nature of the inputs to the discriminator is visualised in Figure 5.

Although presenting the normalised differences to the discriminator resulted in improvements to the training, we did not pass the normalised resistances as inputs to the generator, in order to alleviate the need for more than one initial data point to condition the generator, allowing it to output a sample from a conditional distribution (and subsequent recurrently evaluated samples) given a single resistance conditioning value r_{init} . In the generation of resistance series, we use no state variable, conditioning the generator only on the previous resistance value, implicitly incorporating the inductive bias that the resistance series are memoryless. The generator input is thus a pair of scalar variables representing a normalised resistance and a delay condition. Respectively, we apply an inverse difference normalisation transform at the output of the generator, along with a residual connection to

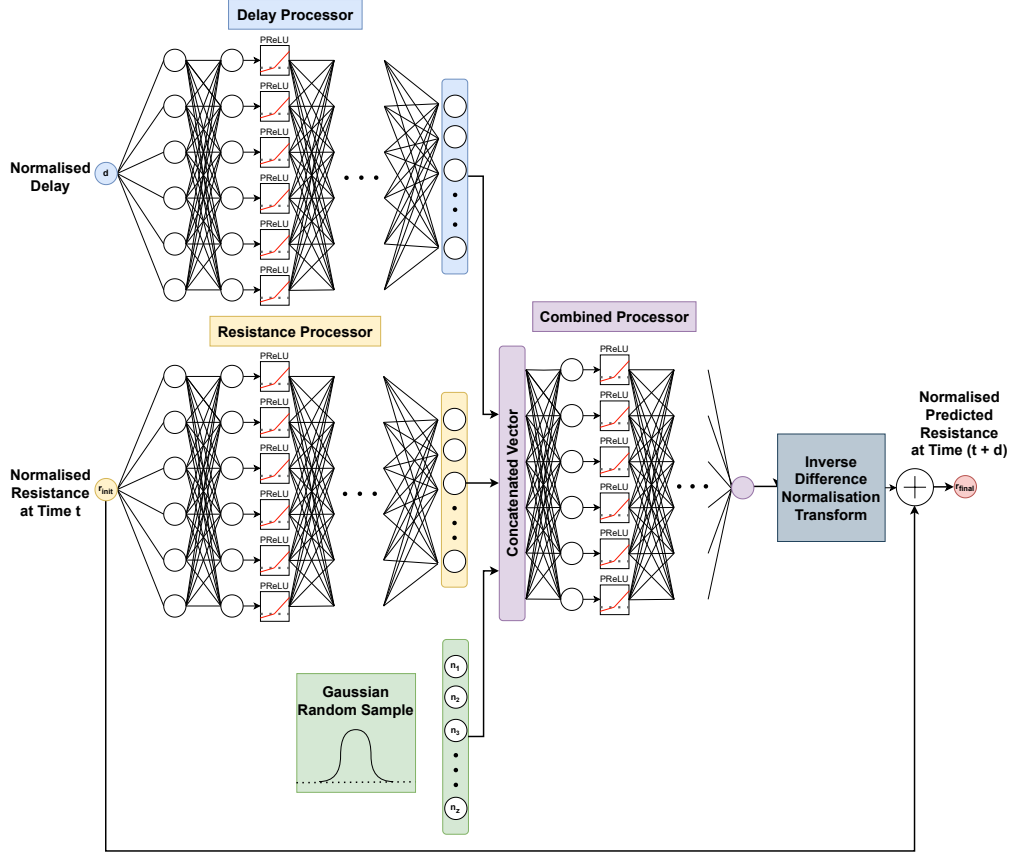


Figure 4: Structure of the cGAN used for training. The delay processor and resistance processor map the delay d and the normalised resistance at time t , denoted by \bar{r}_{init} , to independent embeddings. The combined processor network then processes these embeddings along with the diagonal Gaussian noise vector of dimension z , which is the latent prior for the generative model. The output of the combined processor is a normalised difference, to which the inverse difference normalisation transform is applied, followed by addition to \bar{r}_{init} to produce the predicted resistance after delay d , \bar{r}_{final} .

add the resultant difference to the normalised input resistance to produce a normalised generated final resistance. The dimensionality and nature of the inputs to the generator can be seen in Figure 4.

3.4.3 Multiple Sample Discrimination

One notable challenge that plagues the training of GANs is the problem of mode collapse [Arjovsky and Bottou, 2016]. In our case, the problem presents itself as a tendency for the network to accurately learn the mean value of the resistance changes, but to learn a variance that is smaller than that of the true conditional distribution.

In order to improve the discriminator’s effectiveness at identifying this phenomenon in an attempt to alleviate mode collapse, we pass n real or generated sequences jointly to the discriminator as input. Thus, our effective batch size is reduced from its initial value b to b/n for the discriminator. This technique has been previously demonstrated to improve training by addressing the problem of mode collapse [Lin et al., 2020, Salimans et al., 2016].

The disadvantage of this technique, in addition to the reduction in the size of the batch, is that it increases the effective dimensionality of the discriminator input. We must therefore trade-off these disadvantages for the reduced level of mode-collapse observed with this increased computational complexity. In practice, we find that a value of $n = 2$ produces good results and that is the setting used for the results presented in Section 4.

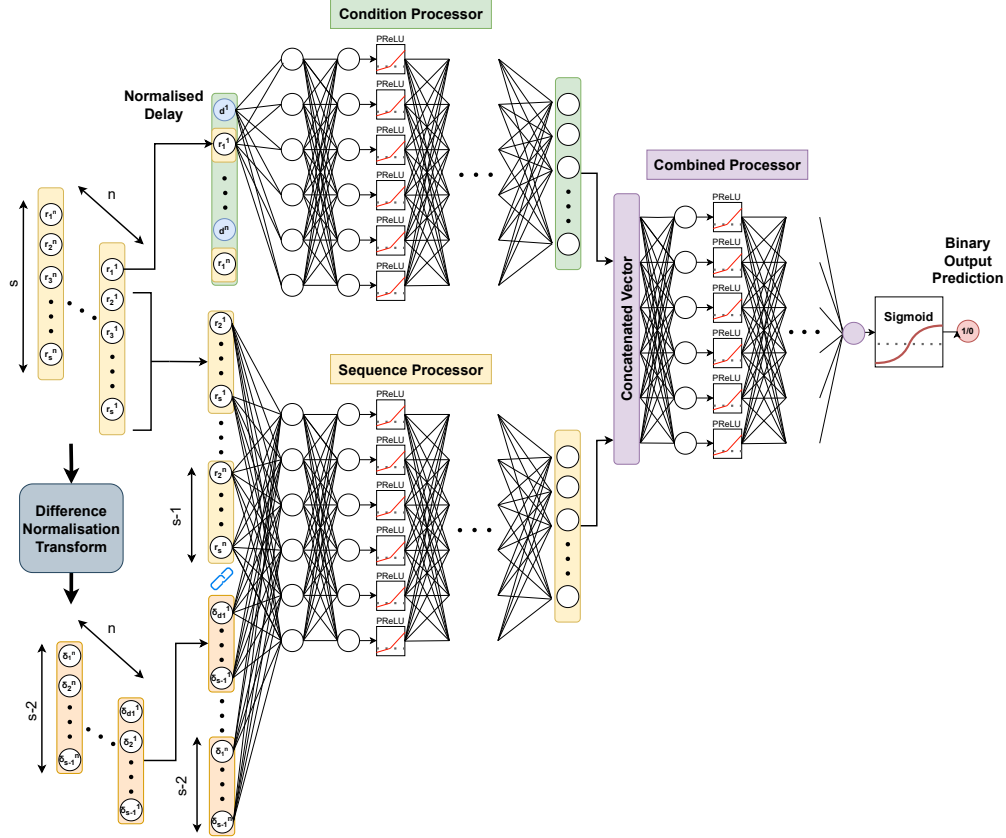


Figure 5: The discriminator architecture and the multiple sample discrimination approach. The condition processor processes the first element of the sequence, i.e., the initial condition, in addition to the delay. The remaining elements of the sequence vector: $r_2 \dots r_s$, are passed to the sequence processor, along with the output of the difference normalisation transform applied to each sequence. The output embeddings of both processors are concatenated and passed to the combined processor. When using the technique of multiple sample discrimination, we pass n sequences (and n delays) to the network simultaneously, with the condition processor and sequence processor input dimensions being scaled up by n and the effective batch size for the discriminator scaled down by n . The same architecture is used for the main and auxiliary delay discriminators described in Section 3.1.

This technique is applied to both the main discriminator network, and the auxiliary delay discriminator network, described in Section 3.1. The use of multiple simultaneous samples for input to the discriminator is shown in a diagram depicting the discriminator architecture in Figure 5.

3.4.4 Parameters

We optimise all networks using an Adam optimiser [Kingma and Ba, 2017] with a learning rate of 1×10^{-4} . We set the sequence length for the generation, and also thus the number of resistance values passed to the discriminator in a single sequence, as $s = 10$. We set the sequence length for input to the delay discriminator as $s = 2$ (i.e., a single generation) although, as described in Algorithm 1, the generator is run with either a sequence length of $s = 2$ or a sequence length of $s = 1 + q$ in the case of the delay discriminator, for both the full and split delay settings.

We run each GAN training experiment for 1000 epochs, with each epoch consisting of 500 steps, where all three networks are updated simultaneously. We set the value of $q_{\max} = 20$. The dimension of the latent prior for the generator, denoted by z , is set to 20. We set the minimum and maximum delays for the main discriminator as $d_{\min,d} = 1$ and $d_{\max,d} = 90$, and those for the delay discriminator as $d_{\min,dd} = 1$ and $d_{\max,dd} = 500$.

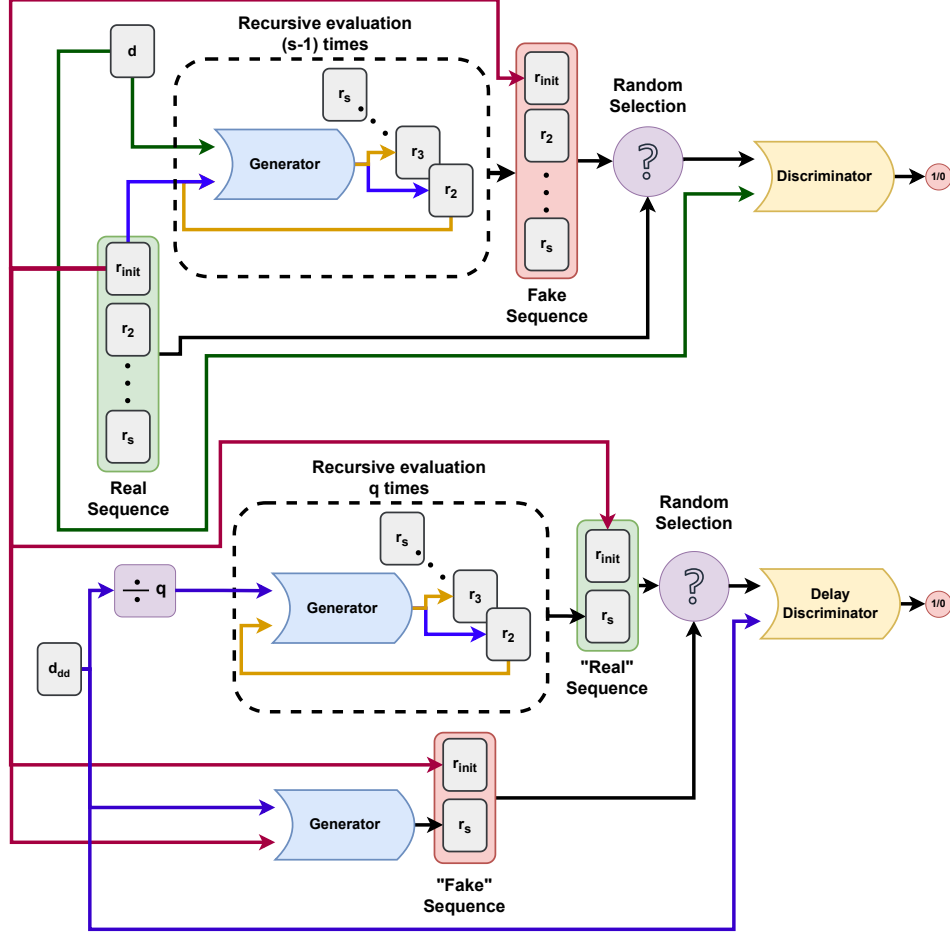


Figure 6: The training structure for the generator and the two discriminators. This visualises the delay discrimination procedure. For the purposes of clarity in visualisation, we do not show multiple sample discrimination in this figure. The top of the diagram shows the generation of a fake sequence for the canonical adversarial training, with the discriminator trained to distinguish between real and fake resistance sequences. The bottom of the diagram shows the training of the cGAN to enforce consistency in its output for the same total delay, also addressing the problems with closed loop training described in Section 3.1.

4 Results

We evaluate the distribution matching performance of the trained generator model, compared to the true distribution of the data in the resistive drift dataset, in several different ways. In order to highlight the consistency of the model output across delays, whose improvement is a key benefit of the delay discriminator approach, we evaluate across a range of equivalent delays using a variety of smaller timesteps. We can also visually compare the series output by the model during closed loop evaluation, which can highlight problems associated with the compounding of closed loop errors and can give some sense of the quality of the generative model. Finally, we compare the statistics of the cGAN model output to those of the ground truth event-based model. We statistically estimate the mean and variance (the first and second order statistical moments) of the generated data, as well as showing empirical model outputs for a variety of combinations of delay and initial resistance conditions.

In order to measure the impact of the techniques used to improve the model training, during evaluation, we also perform an ablation experiment which does not make use of the delay discriminator.

4.1 Delay Consistency Evaluation

Here, we compare the mean difference from the initial resistance at time $t = 0$, for the model run for an equivalent delay of 500, generated by conditioning with a delay condition of (5, 10, 100, 250, and 500), for (1, 2, 5, 50, and 100) recurrent steps, respectively, in order to achieve the same total delay for the model’s final resistance output. We see that the model’s output is relatively consistent across delays. We evaluate this behaviour for experiments run with, and without, the delay discriminator. We find that the delay discriminator improves the consistency of the model outputs for the same total delay for different given delay conditions. This is shown in Figure 7.

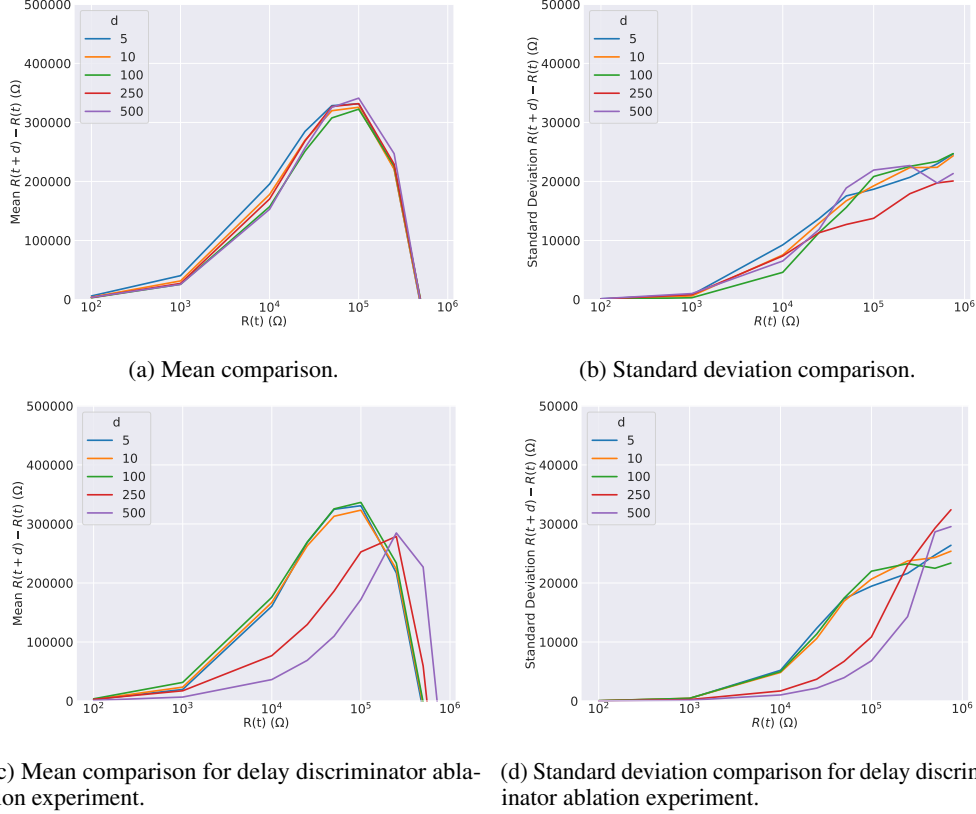


Figure 7: Experiments examining the consistency of the model for generation of outputs of the same cumulative delay, ΔT , at different levels of delay refinement d . We measure the mean change in the resistance for a variety of starting resistance values. In the case of a delay of d , we use $500/d$ steps run in order to achieve a total equivalent delay of $\Delta T = 500$.

4.2 Qualitative Evaluation

Below, we evaluate the model by recurrently generating time series data for a variety of delay conditions. This is done in order to demonstrate the model’s ability to generate visually realistic series for a variety of initial resistance values and conditions, and to exhibit the lack of closed loop errors as part of the recurrent evaluation. We generate 20 series for each initial resistance value for a range of initial resistance values (for any given delay). In each case, we generate for a number of steps equal to $\lceil (1000 + d)/d \rceil$, where d is the delay condition. Example series generations are shown for the delay conditions of 1, 10, 100, 500 in Figure 8. These can be compared to the real series in the dataset, shown in Figure 1, showing that the network has learnt to match the equilibrium point of convergence of $500k\Omega$ for a range of delay conditions and initial resistance values.

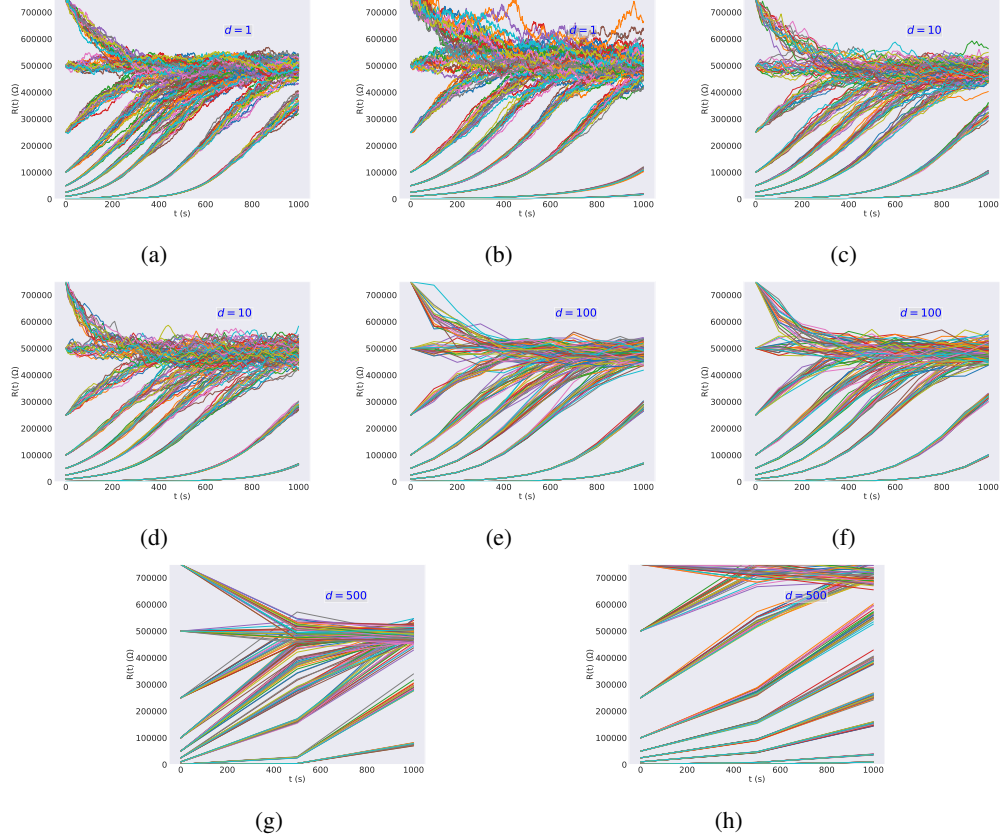


Figure 8: Generated series for different delays with (left figures 8a, 8c, 8e, 8g) and without (right figures 8b, 8d, 8f, 8h) the delay discriminator, for an equivalent delay of 1000, recurrently evaluated for different delay conditions $d \in \{1, 10, 100, 500\}$.

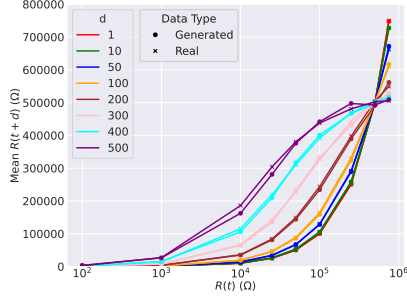
4.3 Conditioned Statistics Evaluation

In Figure 9, we present a comparison of the statistical means and standard deviations of the learned conditional distribution to those estimated from the real model. In order to estimate these statistics, we generate 100 samples of the cGAN model output for each set of conditions, and do the same for the ground truth event-based model (also using 100 samples per parameter estimate). We plot comparisons for both the proposed cGAN model, and for an ablation experiment excluding the delay discriminator.

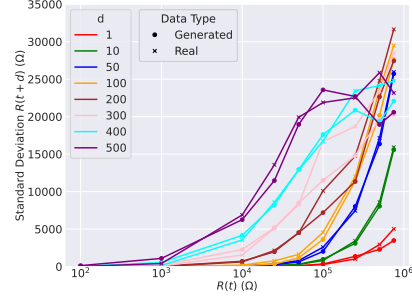
Figure 10a shows final resistance values for given initial resistance and delay conditions, simulated using the true event-based model (the ground truth). Figure 10b shows a comparison of the final resistance values for the same conditions, with simulations performed by the cGAN model. For delays, ΔT , up to $\Delta T = 500s$, which was the maximum value of d_{dd} (the delay discriminator delay), we see that the model's performance is accurate. Although, for delays above this (1000s) the cGAN model's similarity to the true statistics drops.

Figure 10c shows the model output for the same conditions, but using a recurrent evaluation with a delay of $d = \Delta T/10$, for 10 closed loop recursions (feeding the output of the model back to itself as input). We see that recurrently evaluating the model with a smaller delay enables more accurate recreation of the statistics for this larger total delay.

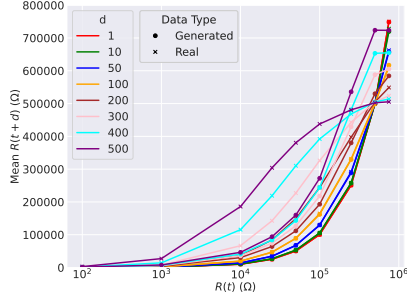
We see, in Figure 10d, the model output for the same conditions, for an ablation experiment run without the delay discriminator. The same recurrent evaluation setting for the delay discriminator is shown in Figure 10e. As can be seen, the model's accuracy in matching the statistics of the dataset for delays larger than those in the training data (i.e., $d_{\max} = 90s$) is significantly degraded. When the generator is evaluated recurrently, we see an improved performance, due to the presence of these



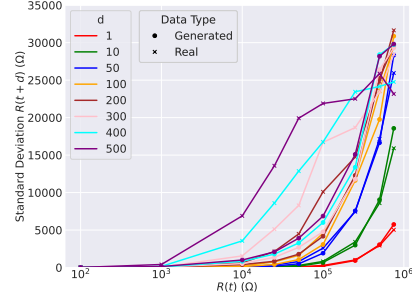
(a) Mean comparison.



(b) Standard deviation comparison.



(c) Mean comparison for delay discriminator ablation experiment.



(d) Standard deviation comparison for delay discriminator ablation experiment.

Figure 9: Means and standard deviations of the final resistance conditioned on different combinations of initial resistances and delays, for the generator trained using the delay discriminator (Figure 9a and 9b) and trained without the delay discriminator as an ablation experiment (Figures 9c and 9d). The empirical statistics for each condition are plotted alongside those obtained from the ground truth model, in order to demonstrate the ability of the model to fit to the true distribution. We see a marked improvement in the statistical moment matching when using the delay discriminator. Legend entries denote the delay, d that the statistics are evaluated for, with ‘real’ entries being the statistics derived from the ground truth event-based model.

smaller delay conditions in the training data. The fact that more accurate modelling for larger delays requires recurrent evaluation using smaller delays in the absence of delay discrimination, justifies the use of delay discrimination in enabling computationally simple conditional distribution modelling for larger delays.

5 End-to-End Quantisation Level Optimisation

In order to demonstrate the advantages of our proposed generative modelling approach in the context of end-to-end learning, we here present an application of the differentiable model for the optimisation of quantisation levels and decoding boundaries for multilevel data storage on memristors. Here, the differentiable nature of the model is crucial in enabling optimisation of quantisation parameters using gradient descent. The computational efficiency in simulating outputs for large delay conditions - without the need for recurrent evaluation - enables fast Monte Carlo estimation of statistical parameters of interest, which can be used to improve the quantisation parameters using accurate error estimates derived from large numbers of samples, without problems associated with vanishing gradients.

5.1 Problem Statement

We consider the problem of storing discrete values on a noisy memristor, making use of the cGAN model as a differentiable storage model that can be used for optimisation of the quantisation levels and boundaries, providing an automated method for selection of a storage and threshold decoding approach.

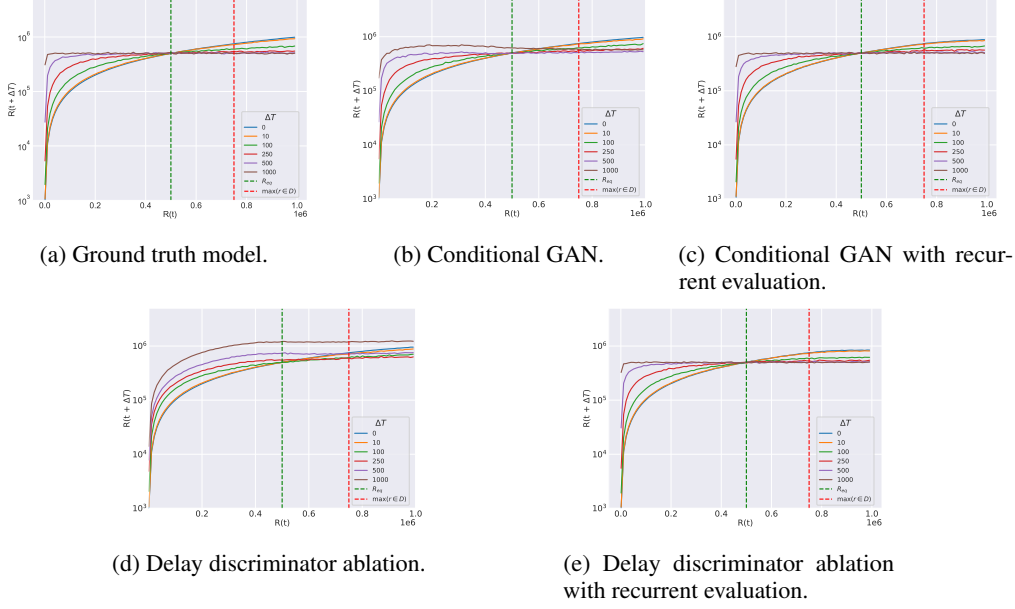


Figure 10: Empirically sampled final resistance values for given initial resistance and delay values. Figures 10a and 10b show the statistics for the ground truth event-based model and cGAN, respectively. Figure 10c shows statistics for cGAN evaluated recurrently with a delay of $d/10$ and 10 recurrent steps. Figure 10d shows an ablation experiment run without the delay discriminator, and Figure 10e shows a recurrent evaluation of the delay discriminator ablation experiment with a delay of $d/10$ and 10 recurrent steps.

Let \mathcal{L} denote an ordered set of quantisation levels, and \mathcal{B} , where $B[0] \triangleq -\infty$ and $B[|B|] \triangleq \infty$, denote an ordered set of quantisation boundaries. Note that the decoding boundaries for the i 'th quantisation level, l_i , which border the bin, are defined as the half-open interval $[B[i], B[i+1])$. We consider the problem of maximising the number of quantisation levels, $|\mathcal{L}|$, that can be decoded given a maximum tolerable threshold on the probability of error, ϵ , based on the decoding approach defined by \mathcal{B} :

$$\max_{\mathcal{L}, \mathcal{B}} |\mathcal{L}| \quad \text{s.t.} \quad \frac{1}{|\mathcal{L}|} \sum_{l_i \in \mathcal{L}} \mathbb{E} [\mathbf{1}_{[B[i], B[i+1])} (G(l_i, d))] \leq \epsilon \quad (10)$$

where d is the chosen delay, $\mathbf{1}_A$ is the indicator function, and $G(r, d)$ is the delay and initial resistance conditional resistive drift distribution. Note that here, we have formulated the problem using the cGAN generator as a variational approximation of the true conditional distribution in order to make the problem differentiable and optimisable through gradient descent, as well as enabling quick Monte Carlo estimation of the average decoding error.

5.2 Method

We use a stochastic gradient descent approach to optimise the quantisation levels and decoding boundaries. Our loss consists of three terms:

1. **Crossover loss:** Monte-Carlo estimate of integral of the probability density falling outside the given interval, for each distribution marginalised over each of the levels $l_i \in \mathcal{L}$ as an initial resistance value.
2. **Ordering regularisation:** We require that the order of the quantisation bins and their respective boundaries be strictly preserved through penalising any violation of the ordering with a squared error. We enforce the requirement that quantisation levels must lie within their decoding boundaries.

3. **Dynamic range regularisation:** We specify an allowable range - $[r_{\text{qmin}}, r_{\text{qmax}}]$ - for the quantisation levels, ensuring that the upper and lower quantisation levels do not fall outside the boundaries of this range, through a squared error penalty.

We note that the loss function as given is non-zero only if there is an error in the decoding process, or a boundary violation. In the absence of such conditions, the gradient with respect to the quantisation levels and decoding boundaries will be zero. In order to avoid the problem of zero gradients for the regularisation terms when ordering and dynamic range constraints are satisfied, or when the probability of error is low, we use a margin, ρ , such that the loss is non-zero close to points of constraint violation.

Let $h(x, y) \triangleq (\min(x - y, 0))^2$. We can define our loss function for a given delay, L_d , as follows for the margin:

$$\begin{aligned} L_d(\mathcal{L}, \mathcal{B}) := & \sum_{l_i \in \mathcal{L}} \mathbb{E} [h(\mathcal{B}[i] + \rho, G(l_i, d)) + h(G(l_i, d) + \rho, \mathcal{B}[i + 1])] \\ & + \lambda_1 \sum_{l_i \in \mathcal{L}} h(\mathcal{B}[i] + \rho, l_i) + h(l_i + \rho, \mathcal{B}[i + 1]) \\ & + \lambda_2 (h(r_{\text{qmin}} + \rho, l_0) + h(l_0 + \rho, r_{\text{qmax}})) \end{aligned} \quad (11)$$

where λ_1 and λ_2 are regularisation factors.

We use an Adam optimiser [Kingma and Ba, 2017] with an initial learning rate of 1×10^{-3} and a learning rate schedule that reduces the learning rate by a factor of 0.9 whenever the empirical loss does not improve for more than 25 optimisation steps. For each step, we estimated the expected value in Equation 11 through a Monte Carlo estimate over 32 trials. We run our algorithm for each delay value and number of quantisation levels until convergence is observed, or for 10,000 steps, whichever is sooner. We set the allowable input range to $[10000, 500000]$. We set $\lambda_1 = 10$ and $\lambda_2 = |\mathcal{L}|/2$ to discourage violation of the constraints, and set $\rho = 0.05$.

5.3 Results

Figure 11 shows the best achieved quantisation scheme for three examples with different delays. We see that for increasing delay, the maximum value of $|\mathcal{L}|$, and thus the number of bits that can be stored, goes down. We can see that the optimisation procedure tends to result in quantisation levels at the lower end of the learned bins. This corresponds to a correction for the predicted resistive drift in the positive direction (towards the equilibrium resistance of $500k\Omega$).

Figure 12 shows the error probability of the optimised levels and decoding boundaries for varying numbers of levels, under different delay conditions. We observe that as the number of quantisation levels increases, so does the error rate. As the delay increases, the delay-conditioned capacity of the memristor for information storage goes down, and it becomes more difficult to achieve quantised storage with a sufficiently low error probability. We see that the error probability approaches $(|\mathcal{L}| - 1)/|\mathcal{L}|$ as the delay becomes significantly large, indicating a total loss of information, with the boundary decoding scheme having no advantage over a random guess.

Successful optimisation of the quantisation levels and decoding boundaries for a range of delay conditions highlights the efficacy of our model in providing a computationally simple and differentiable model of the resistive drift conditional distribution, enabling efficient Monte Carlo simulation of the decoding error probabilities in an end-to-end training setup.

6 Discussion and Conclusion

In an effort to create a GAN that is conditioned directly on the delay condition, we are able to use the technique of delay discrimination to boost the performance and generalisation of the cGAN when evaluating at larger delays, improving consistency across the timescales of generation, and enabling the use of the model for a variety of delay conditions.

We note that an alternative viewpoint treats delay discrimination as a form of generative data augmentation, where we assume that the model is more accurate at generating sequences with delays within the observed data, than for those delays without. We use the model’s own output sequences

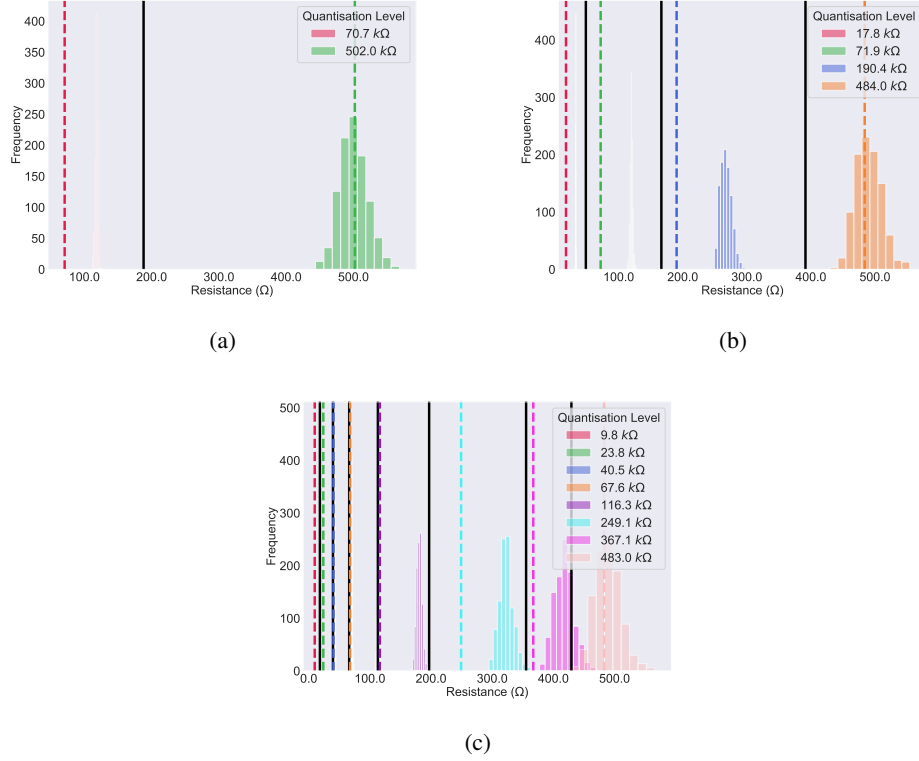


Figure 11: The end-to-end optimised quantisation schemes learned through using the cGAN model as a model of the resistive drift. Figures 11a, 11b, and 11c show the schemes trained for a delay of 100 and 2, 4, and 8 quantisation levels (1, 2, 3 bits), respectively.

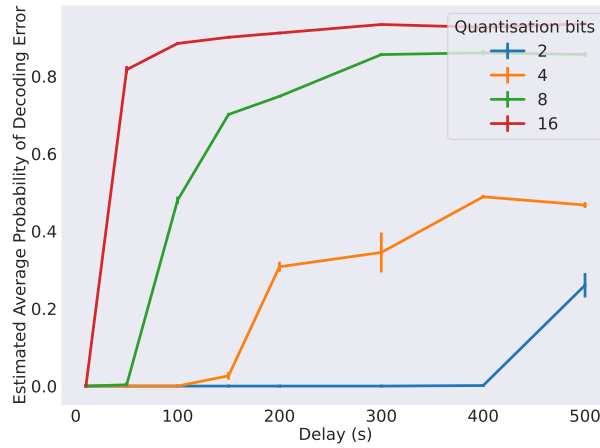


Figure 12: Error vs. delay for different levels of quantisation. As the delay increases, the capacity of the device for storing information decreases, and the decoding error of the optimised quantisation scheme increases, up to a maximum of $(2^b - 1)/2^b$, where b denotes the number of bits of the quantisation scheme. We show results averaged over 5 experiments for each setting.

for smaller delay values, evaluated recurrently, to learn to generate sequences for delay conditions that are much larger than those that would be possible to generate from the finite-length sequences in the dataset.

The cGAN generative model presented is completely memoryless, in the sense that we are assuming that given the current voltage input and the state variable (the resistance), knowledge of previous states of the system would not give any benefit. This may not always be the case however, for example, immediately after a programming pulse, when the volatility may initially be high, but may relax over time, meaning there is dependence on past state or input values [El-Geresy et al., 2024]. It may therefore be desirable to create a model that is able to encapsulate the history of the device state over time and a recurrent or autoregressive network modelling approach may enable the modelling of this behaviour. An approach to doing this in a computationally simple manner is an left as future work. Future work will also include the evaluation of the delay discriminator method more generally, to assess its ability to improve the training performance of generative time series models at a more fundamental level. The modelling approach as presented could also be extended to alternative generative models and architectures, for example, diffusion models [Ho et al., 2020].

Finally, future work could include adapting the modelling approach for a neuromorphic setting, making use the proposed approach for simulations of neuromorphic circuits. In addition, there exists the opportunity to extend the work to an asynchronous setting, for example through the use of spiking neural networks.

Overall, we have demonstrated that it is possible to effectively model the resistive drift phenomenon in memristors through the use of a cGAN trained to model the delay and resistance-conditioned distribution. We saw that we could attempt to tackle multiple challenges associated with the training of adversarial networks for time series data, without the use of supervised losses or scheduled sampling, by making use of a delay discriminator to enforce consistency across a range of timescales. This technique was also shown to extend the scope of the cGAN, for generation of delay-conditioned outputs using a single forward pass, to much larger delays than those present in the dataset.

References

- [Abbey et al., 2022] Abbey, T., Giotis, C., Serb, A., Stathopoulos, S., and Prodromakis, T. (2022). Thermal Effects on Initial Volatile Response and Relaxation Dynamics of Resistive RAM Devices. *IEEE Electron Device Letters*, 43(3):386–389.
- [Arjovsky and Bottou, 2016] Arjovsky, M. and Bottou, L. (2016). Towards Principled Methods for Training Generative Adversarial Networks. In *International Conference on Learning Representations*.
- [Arjovsky et al., 2017] Arjovsky, M., Chintala, S., and Bottou, L. (2017). Wasserstein GAN. In *PMLR*, pages 214–223.
- [Bengio et al., 2015] Bengio, S., Vinyals, O., Jaitly, N., and Shazeer, N. (2015). Scheduled Sampling for Sequence Prediction with Recurrent Neural Networks. In *Advances in Neural Information Processing Systems*, volume 28. Curran Associates, Inc.
- [Berdan et al., 2014] Berdan, R., Lim, C., Khiat, A., Papavassiliou, C., and Prodromakis, T. (2014). A Memristor SPICE Model Accounting for Volatile Characteristics of Practical ReRAM. *IEEE Electron Device Letters*, 35(1):135–137.
- [Carbajal et al., 2015] Carbajal, J. P., Dambre, J., Hermans, M., and Schrauwen, B. (2015). Memristor Models for Machine Learning. *Neural Computation*, 27(3):725–747.
- [Cho et al., 2014] Cho, K., van Merriënboer, B., Gulcehre, C., Bahdanau, D., Bougares, F., Schwenk, H., and Bengio, Y. (2014). Learning Phrase Representations using RNN Encoder–Decoder for Statistical Machine Translation. In Moschitti, A., Pang, B., and Daelemans, W., editors, *Proceedings of the 2014 Conference on Empirical Methods in Natural Language Processing (EMNLP)*, pages 1724–1734, Doha, Qatar. Association for Computational Linguistics.
- [Chua, 1971] Chua, L. (1971). Memristor-The missing circuit element. *IEEE Transactions on Circuit Theory*, 18(5):507–519.
- [Chua, 2011] Chua, L. (2011). Resistance switching memories are memristors. *Applied Physics A*, 102(4):765–783.

- [Chua, 2014] Chua, L. (2014). If it’s pinched it’s a memristor. *Semiconductor Science and Technology*, 29(10):104001.
- [Chua and Sung Mo Kang, 1976] Chua, L. and Sung Mo Kang (1976). Memristive devices and systems. *Proceedings of the IEEE*, 64(2):209–223.
- [Ding et al., 2022] Ding, X., Wang, Y., Xu, Z., Welch, W. J., and Wang, Z. J. (2022). CcGAN: Continuous Conditional Generative Adversarial Networks for Image Generation. In *International Conference on Learning Representations*.
- [El-Geresy et al., 2024] El-Geresy, W., Papavassiliou, C., and Gündüz, D. (2024). Event-Based Simulation of Stochastic Memristive Devices for Neuromorphic Computing. *arXiv:2407.04718 [physics]*.
- [Goodfellow et al., 2014] Goodfellow, I. J., Pouget-Abadie, J., Mirza, M., Xu, B., Warde-Farley, D., Ozair, S., Courville, A., and Bengio, Y. (2014). Generative Adversarial Networks. *Advances in neural information processing systems*.
- [He et al., 2016] He, K., Zhang, X., Ren, S., and Sun, J. (2016). Deep Residual Learning for Image Recognition. In *2016 IEEE Conference on Computer Vision and Pattern Recognition (CVPR)*, pages 770–778.
- [Ho et al., 2020] Ho, J., Jain, A., and Abbeel, P. (2020). Denoising Diffusion Probabilistic Models. In *Advances in Neural Information Processing Systems*, volume 33, pages 6840–6851. Curran Associates, Inc.
- [Hochreiter and Schmidhuber, 1997] Hochreiter, S. and Schmidhuber, J. (1997). Long Short-Term Memory. *Neural Computation*, 9(8):1735–1780.
- [Huszár, 2015] Huszár, F. (2015). How (not) to Train your Generative Model: Scheduled Sampling, Likelihood, Adversary? *arXiv:1511.05101 [cs, math, stat]*.
- [Ielmini, 2011] Ielmini, D. (2011). Modeling the Universal Set/Reset Characteristics of Bipolar RRAM by Field- and Temperature-Driven Filament Growth. *IEEE Transactions on Electron Devices*, 58(12):4309–4317.
- [Kingma and Ba, 2017] Kingma, D. P. and Ba, J. (2017). Adam: A Method for Stochastic Optimization. *arXiv:1412.6980 [cs]*.
- [Lin et al., 2020] Lin, Z., Khetan, A., Fanti, G., and Oh, S. (2020). PacGAN: The Power of Two Samples in Generative Adversarial Networks. *IEEE Journal on Selected Areas in Information Theory*, 1(1):324–335.
- [Malik et al., 2022] Malik, A., Papavassiliou, C., and Stathopoulos, S. (2022). An Absorbing Markov Chain Model for Stochastic Memristive Devices. In *2022 11th International Conference on Modern Circuits and Systems Technologies (MOCASST)*, pages 1–4.
- [Mead, 1990] Mead, C. (1990). Neuromorphic electronic systems. *Proceedings of the IEEE*, 78(10):1629–1636.
- [Mirza and Osindero, 2014] Mirza, M. and Osindero, S. (2014). Conditional Generative Adversarial Nets. *arXiv:1411.1784 [cs, stat]*.
- [Molter and Nugent, 2016] Molter, T. W. and Nugent, M. A. (2016). The Generalized Metastable Switch Memristor Model. In *CNNA 2016; 15th International Workshop on Cellular Nanoscale Networks and Their Applications*, pages 1–2.
- [Oh et al., 2019] Oh, S., Huang, Z., Shi, Y., and Kuzum, D. (2019). The Impact of Resistance Drift of Phase Change Memory (PCM) Synaptic Devices on Artificial Neural Network Performance. *IEEE Electron Device Letters*, 40(8):1325–1328.
- [Pickett et al., 2009] Pickett, M. D., Strukov, D. B., Borghetti, J. L., Yang, J. J., Snider, G. S., Stewart, D. R., and Williams, R. S. (2009). Switching dynamics in titanium dioxide memristive devices. *Journal of Applied Physics*, 106(7):074508.
- [Ronneberger et al., 2015] Ronneberger, O., Fischer, P., and Brox, T. (2015). U-Net: Convolutional Networks for Biomedical Image Segmentation. In Navab, N., Hornegger, J., Wells, W. M., and Frangi, A. F., editors, *Medical Image Computing and Computer-Assisted Intervention – MICCAI 2015*, Lecture Notes in Computer Science, pages 234–241, Cham. Springer International Publishing.

- [Rumsey, 2019] Rumsey, S. (2019). *Capacity Considerations for Data Storage in Memristor Arrays*. PhD thesis, University of Toronto, Toronto, Canada.
- [Salimans et al., 2016] Salimans, T., Goodfellow, I., Zaremba, W., Cheung, V., Radford, A., and Chen, X. (2016). Improved Techniques for Training GANs. *arXiv:1606.03498 [cs]*.
- [Strukov et al., 2008] Strukov, D. B., Snider, G. S., Stewart, D. R., and Williams, R. S. (2008). The missing memristor found. *Nature*, 453(7191):80–83.
- [Sung et al., 2018] Sung, C., Hwang, H., and Yoo, I. K. (2018). Perspective: A review on memristive hardware for neuromorphic computation. *Journal of Applied Physics*, 124(15):151903.
- [van den Oord et al., 2016] van den Oord, A., Dieleman, S., Zen, H., Simonyan, K., Vinyals, O., Graves, A., Kalchbrenner, N., Senior, A., and Kavukcuoglu, K. (2016). WaveNet: A Generative Model for Raw Audio. *arXiv:1609.03499 [cs]*.
- [Vaswani et al., 2017] Vaswani, A., Shazeer, N., Parmar, N., Uszkoreit, J., Jones, L., Gomez, A. N., Kaiser, Ł., and Polosukhin, I. (2017). Attention is all you need. In *Proceedings of the 31st International Conference on Neural Information Processing Systems, NIPS’17*, pages 6000–6010, Red Hook, NY, USA. Curran Associates Inc.
- [Williams et al., 2013] Williams, R. S., Pickett, M. D., and Strachan, J. P. (2013). Physics-based memristor models. In *2013 IEEE International Symposium on Circuits and Systems (ISCAS)*, pages 217–220.
- [Yang et al., 2008] Yang, J. J., Pickett, M. D., Li, X., Ohlberg, D. A. A., Stewart, D. R., and Williams, R. S. (2008). Memristive switching mechanism for metal/oxide/metal nanodevices. *Nature Nanotechnology*, 3(7):429–433.
- [Yoon and Jarrett, 2019] Yoon, J. and Jarrett, D. (2019). Time-series Generative Adversarial Networks. *Advances in Neural Information Processing Systems*, pages 5508–5518.
- [Zarcone et al., 2020] Zarcone, R. V., Engel, J. H., Burc Eryilmaz, S., Wan, W., Kim, S., BrightSky, M., Lam, C., Lung, H.-L., Olshausen, B. A., and Philip Wong, H.-S. (2020). Analog Coding in Emerging Memory Systems. *Scientific Reports*, 10(1):6831.